ChemComm

A porous supramolecular ionic solid

Journal:	*ChemComm*
Manuscript ID	CC-COM-05-2021-002806.R2
Article Type:	Communication

COMMUNICATION

A porous supramolecular ionic solid

Nathan Jackson,[b] Irma Rocio Vazquez,[b] Ying-Pin Chen,[c] Yu-Sheng Chen[c] and Wen-Yang Gao*[a]

Received 00th January 20xx,
Accepted 00th January 20xx

DOI: 10.1039/x0xx00000x

We report a synthetic strategy to integrate discrete coordination cages into extended porous materials by decorating opposite charges on the singular cage, which offers multidirectional electrostatic forces among cages and leads to a porous supramolecular ionic solid. The resulting material is non-centrosymmetric and affords a piezoelectric coefficient of 8.19 pC/N, higher than that of the wurtzite ZnO.

Discrete coordination cages, also known as metal-organic cages or metal-organic polyhedra, constructed by the self-assembly of metal ion or clusters and organic ligands,[1-3] have recently garnered significant attention as a class of permanently porous materials.[4-6] Structural designability and modularity, similar to that of MOFs,[7,8] along with solution processibility, enable families of coordination cages to be investigated in gas storage/separation,[9] catalysis,[10,11] and drug delivery.[12] Given their large internal cavities and tunable diversified structures, coordinate cages have been viewed as supramolecular building blocks to build infinite porous framework materials.[13-15] In order to achieve the extended frameworks, two well-known strategies[16] have been investigated: 1) pillaring linkers to bridge unsaturated metal sites of coordination cages (Figure 1a);[17-19] 2) mechanical bonds, including interlocking and interpenetrating, to expand the dimension (Figure 1b).[20-22] Recently, Bloch et al. reported an example of porous ionic solids based on the self-assembly of two different types of coordination cages carrying oppositely charges (Figure 1c).[23]

Herein, we report a new synthetic strategy of decorating charges on the building blocks (e.g., organic ligands), which results into charge separation on the singular coordination cage and enables to extend coordination cages into a permanently porous material. An ionic solid is composed of cations and anions held together by electrostatic forces. Our strategy introduces opposite charges to separated sites of the singular supramolecular coordination cage, which offers

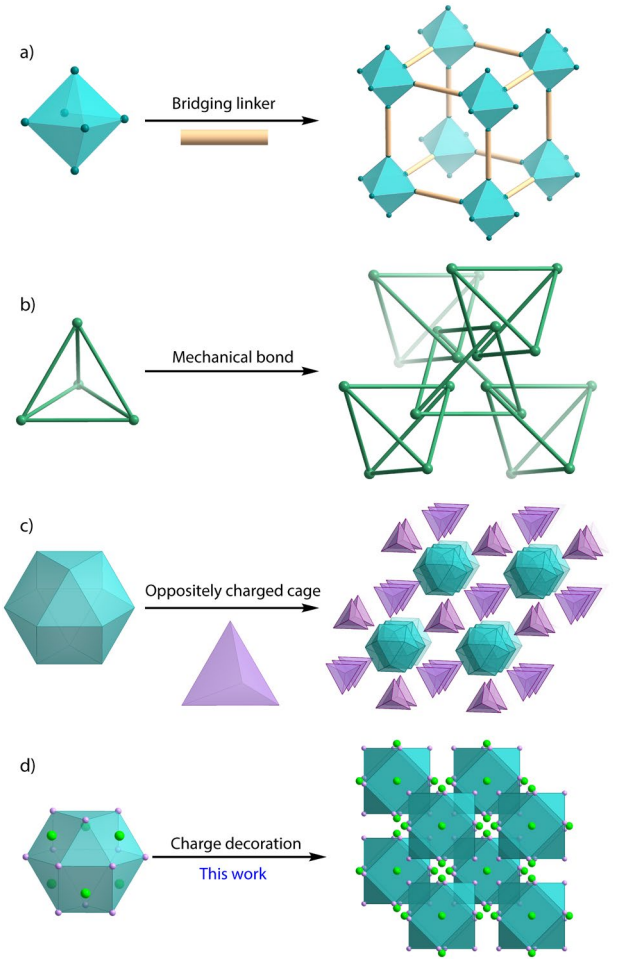

Figure 1. a) Pillaring linkers are added to bridge unsaturated metal sites of discrete coordination cages (● unsaturated metal sites). b) Mechanical bonds, such as interlocking and interpenetrating, are built to extend the frameworks. c) Electrostatic forces between oppositely charged coordination cages construct a porous material. d) Here we report that electrostatic forces between different sites of the singular cage (●,● sites carrying opposite charges) build a porous supramolecular ionic solid.

[a] *Department of Chemistry, New Mexico Institute of Mining and Technology, Socorro, New Mexico 87801, United States. E-mail: wenyang.gao@nmt.edu*
[b] *Department of Mechanical Engineering, University of New Mexico, Albuquerque, New Mexico 87106, United States.*
[c] *NSF's ChemMatCARS, The University of Chicago, Lemont, Illinois 60439, United States.*

† Electronic Supplementary Information (ESI) available: Experimental details, spectra, X-ray crystallographic information, and additional figures and tables. CCDC 2085461. For ESI and crystallographic data in CIF see DOI: 10.1039/x0xx00000x

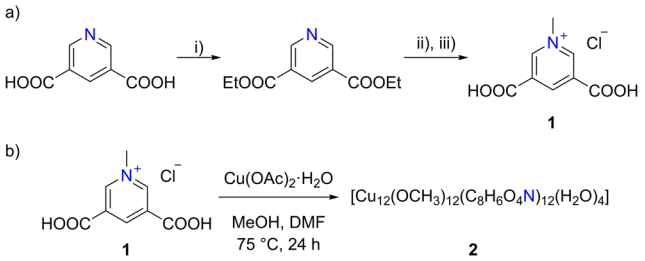

Figure 2. a) The synthetic steps of 3,5-dicarboxy-1-methylpyridinium chloride (**1**). Conditions: i) EtOH, H_2SO_4, 78 °C, 24 h. ii) MeI, toluene, MeCN, 65 °C, 24 h. iii) HCl, 90°C, 72 h. b) Solvothermal reaction of 1 and $Cu(OAc)_2{\cdot}H_2O$ affords blue blocked-shaped crystals of **2**.

multidirectional electrostatic forces among cages and leads to an ordered close-packing supramolecular ionic solid (Figure 1d).

We initiated these investigations by choosing an organic ligand featuring a motif (e.g., pyridine-3,5-dicarboxylic acid) resembling isophthalic acid, commonly encountered in the assembly of coordination cages.[24,25] Meanwhile, to exemplify the proof-of-concept, we employed the *N*-methylation of pyridine via iodomethane to introduce the positive charge to the ligand. Therefore, we synthesized 3,5-dicarboxy-1-methylpyridinium chloride (**1**) as the ligand (Figure 2a), starting from pyridine-3,5-dicarboxylic acid followed by esterification, *N*-methylation, and hydrolysis (see details in Supporting Information). The solvothermal reaction of **1** and $Cu(OAc){\cdot}H_2O$ in the presence of *N,N*-dimethylformamide (DMF) and methanol at 75 °C for 24 hours provides blue block-shaped crystals of **2** (Figure 2b). In contrast, the same reaction condition with pyridine-3,5-dicarboxylic acid, instead of **1**, does not afford any crystalline phase (Figure S1).

Single-crystal X-ray diffraction (SCXRD) analysis reveals that **2** crystallizes in the cubic space group of $I\bar{4}3m$ (a = 20.746(3) Å, Table S1) with an empirical formula of $[Cu_{12}(OCH_3)_{12}(C_8H_6O_4N)_{12}(H_2O)_4]$. As shown in Figures 3a and 3b, the metal cluster is composed of two square-pyramidal Cu(II) cations bridged by two μ_2-methoxide anions. While an aqua ligand partially occupies the axial position of the square pyramid pointing toward the inside, each Cu(II) also coordinates with two oxygen atoms of two carboxylate groups from different ligands in a *cis* mode, which generates a basal plane with two oxygen atoms of the methoxide ions. Overall, each metal cluster with a formula of $[Cu_2(OMe)_2(OOC)_4(H_2O)_{0.7}]^{2-}$ (Figure 3b) carries two negative charges. Each positively charged pyridinium moiety connects two metal clusters via the carboxylate groups. Thus, the discrete coordination cage is constructed by six negatively charged metal clusters (including twelve methoxide anions and aqua ligands, respectively) and twelve positively charged organic ligands (Figure 3a). A cuboctahedron can be generated by connecting the twelve positively charged nitrogen sites, while the six negatively charged metal clusters are distributed at the centres of the six square faces (Figure 3c). Separated charge distribution at the vertices or on the faces of the polyhedron directs the packing of the coordination cages in the 3-dimensional space. The multidirectional electrostatic

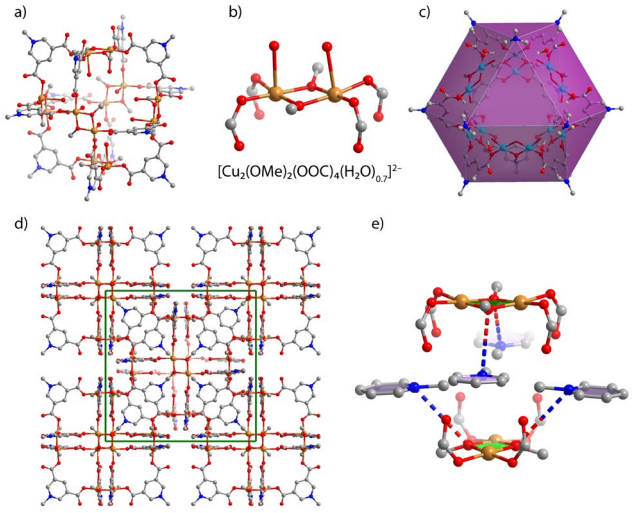

Figure 3. a) The discrete coordination cage, **2**, is built from the solvothermal reaction of **1** and $Cu(OAc)_2{\cdot}H_2O$. b) The metal cluster, $[Cu_2(OMe)_2(OOC)_4(H_2O)_{0.7}]^{2-}$, carries negative charges. c) A cuboctahedron is formed by connecting the twelve positively charged nitrogen sites and the six negatively charged metal clusters are distributed at the centres of the six square faces of the cuboctahedron. d) The discrete cages follow a body-centred cubic packing mode. e) The electrostatic forces between different sites in the ionic solid are illustrated by dotted lines, drawn by the positive sites and their closest negative sites (the axial aqua ligands were omitted for clarity).

forces between cages result in a supramolecular ionic solid with a body-centred cubic packing (Figure 3d). The electrostatic forces between different sites in the ionic solid are illustrated in Figure 3e.

Powder X-ray diffraction (PXRD) analysis verifies the phase purity of **2**, based on the agreement between the experimental patterns and the calculated ones (Figure S2). Meanwhile, the obtained supramolecular ionic solid, **2**, exhibits distinctive chemical stability after being soaked for one week in a series of different organic solvents, e.g., acetonitrile (MeCN), acetone, dichloromethane (CH_2Cl_2), methanol (MeOH), and tetrahydrofuran (THF), probed by PXRD patterns (Figure 4a). In addition, the desolvated sample obtained by extensive acetonitrile exchange and evacuation at 90 °C still demonstrates consistent PXRD patterns (Figure S2), compared with the initial ones.

Based on these observations, **2** was activated by exhaustive acetonitrile exchange followed by heating at 90 °C under vacuum prior to gas adsorption analysis. The permanent porosity of **2** was characterized by N_2 adsorption isotherms at 77K (Figure 4b), which provided a measured Brunauer-Emmett-Teller (BET) surface area of 690 m^2/g (P/P_0 = 0.02–0.15). Though the multidirectional electrostatic forces lead to a close-packing solid of **2**, it still exhibits permanent porosity due to the empty internal space of coordination cages and their ordered packing (Figure S3).

Piezoelectric materials, which convert mechanical stress into electrical energy (and *vice versa*), are crucial in energy storage, sensors, actuators, and others.[26,27] Given the non-centrosymmetric space group and the remarkable chemical stability of **2**, we examined its piezoelectric response using a Berlincourt piezometer (details in Supporting Information).

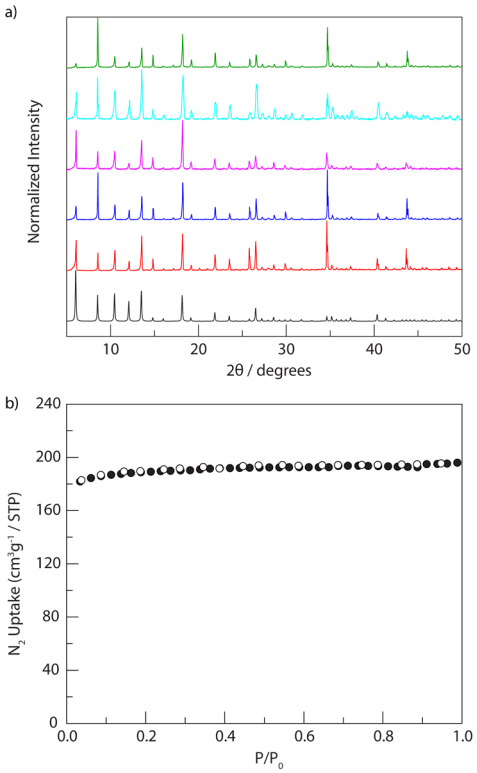

Figure 4. a) Compared with its calculated PXRD pattern (—), **2** shows consistent PXRD patterns after being soaked for one week in a series of organic solvents, including MeCN (—), acetone (—), CH_2Cl_2 (—), MeOH (—), and THF (—). b) N_2 adsorption isotherms of **2** (adsorption (●), desorption (○)) were measured at 77 K. Its Brunauer-Emmett-Teller (BET) surface area was generated with a value of 690 m^2/g (P/P_0 = 0.02–0.15).

Multiple measurements provide an average piezoelectric coefficient, d_{33} value, of 8.19 (±1.30) pC/N. To validate the measurement, the same analysis method provides a d_{33} value of 4.30 pC/N for the wurtzite zinc oxide (ZnO) powder, consistent with the reported value on ZnO in the range of 3 – 12 pC/N.[28] To the best of our knowledge, **2** represents the first coordination cage reported with a piezoelectric response, which may expand the scope of well-explored traditional piezoelectric materials.

In conclusion, we report a new synthetic strategy of charge decoration to extend discrete coordination cages into a supramolecular ionic solid. While multidirectional electrostatic forces between positively charged ligands and negatively charged metal nodes among cages lead to a close packing, the empty internal space of the coordination cage still provides the permanent porosity of the resultant solid. Meanwhile, we describe its piezoelectric response, which outperforms that of the ZnO powder. The emerging metal-organic materials may provide promising potentials as a new class of piezoelectric materials, in addition to the well-known pure inorganic materials.

Acknowledgements

W. Y. G. acknowledges the start-up fund of New Mexico Tech. N. J. acknowledges partial support from U.S. Department of Defense (DoD) Army Research Office (No. 76064-RT-RFP). Single-crystal data of **2** were acquired at NSF's ChemMatCARS. NSF's ChemMatCARS Sector 15 is supported by the Divisions of Chemistry (CHE) and Materials Research (DMR), National Science Foundation, under grant number NSF/CHE-1834750. Use of the Advanced Photon Source, an Office of Science User Facility operated for the U.S. Department of Energy (DOE) Office of Science by Argonne National Laboratory, was supported by the U.S. DOE under Contract No. DE-AC02-06CH11357. We thank Junyu Ren (University of North Texas) for the thermogravimetric analysis.

There are no conflicts to declare.

References

1 T. R. Cook and P. J. Stang, *Chem. Rev.*, 2015, **115**, 7001.
2 M. M. Smulders, I. A. Riddell, C. Browne and J. R. Nitschke, *Chem. Soc. Rev.*, 2013, **42**, 1728.
3 M. Han, D. M. Engelhard and G. H. Clever, *Chem. Soc. Rev.*, 2014, **43**, 1848.
4 M. M. Deegan, A. M. Antonio, G. A. Taggart and E. D. Bloch, *Coord. Chem. Rev.*, 2021, **430**, 213679.
5 A. J. Gosselin, C. A. Rowland and E. D. Bloch, *Chem. Rev.*, 2020, **120**, 8987.
6 S. Mollick, S. Fajal, S. Mukherjee and S. K. Ghosh, *Chem. Asian J.*, 2019, **14**, 3096.
7 H. Furukawa, K. E. Cordova, M. O'Keeffe and O. M. Yaghi, *Science*, 2013, **341**, 1230444.
8 H. C. Zhou and S. Kitagawa, *Chem. Soc. Rev*, 2014, **43**, 5415.
9 J. R. Li and H. C. Zhou, *Nat. Chem.*, 2010, **2**, 893.
10 C. M. Hong, R. G. Bergman, K. N. Raymond and F. D. Toste, *Acc. Chem. Res.*, 2018, **51**, 2447.
11 W.-X. Gao, H.-N. Zhang and G.-X. Jin, *Coord. Chem. Rev.*, 2019, **386**, 69.
12 D. Zhao, S. Tan, D. Yuan, W. Lu, Y. H. Rezenom, H. Jiang, L.-Q. Wang and H.-C. Zhou, *Adv. Mater.*, 2011, **23**, 90.
13 J. J. Perry IV, J. A. Perman and M. J. Zaworotko, *Chem. Soc. Rev.*, 2009, **38**, 1400.
14 F. Nouar, J. F. Eubank, T. Bousquet, L. Wojtas, M. J. Zaworotko and M. Eddaoudi, *J. Am. Chem. Soc.*, 2008, **130**, 1833.
15 A. J. Cairns, J. A. Perman, L. Wojtas, V. C. Kravtsov, M. H. Alkordi, M. Eddaoudi and M. J. Zaworotko, *J. Am. Chem. Soc.*, 2008, **130**, 1560.
16 L. Chen, Q. Chen, M. Wu, F. Jiang and M. Hong, *Acc. Chem. Res.*, 2015, **48**, 201.
17 H. N. Wang, X. Meng, G. S. Yang, X. L. Wang, K. Z. Shao, Z. M. Su and C. G. Wang, *Chem. Commun.*, 2011, **47**, 7128.
18 E. J. Gosselin, G. R. Lorzing, B. A. Trump, C. M. Brown and E. D. Bloch, *Chem. Commun.*, 2018, **54**, 6392.
19 J.-R. Li, D. J. Timmons and H.-C. Zhou, *J. Am. Chem. Soc.*, 2009, **131**, 6368.
20 L. Jiang, P. Ju, X. R. Meng, X. J. Kuang and T. B. Lu, *Sci. Rep.*, 2012, **2**, 668.
21 X. Kuang, X. Wu, R. Yu, J. P. Donahue, J. Huang and C.-Z. Lu, *Nat. Chem.*, 2010, **2**, 461.
22 J. Heine, J. S. auf der Günne and S. Dehnen, *J. Am. Chem. Soc.*, 2011, **133**, 10018.
23 E. J. Gosselin, G. E. Decker, A. M. Antonio, G. R. Lorzing, G. P. A. Yap and E. D. Bloch, *J. Am. Chem. Soc.*, 2020, **142**, 9594.
24 B. Moulton, J. Lu, A. Mondal and M. J. Zaworotko, *Chem. Commun.*, 2001, 863.
25 M. Eddaoudi, J. Kim, J. B. Wachter, H. K. Chae, M. O'Keeffe and O. M. Yaghi, *J. Am. Chem. Soc.*, 2001, **123**, 4368.
26 M. Safaei, H. A. Sodano and S. R. Anton, *Smart Mater. Struct.*, 2019, **28**, 113001.

27 H. Liu, J. Zhong, C. Lee, S.-W. Lee and L. Lin, *Appl. Phys. Rev.*, 2018, **5**, 041306.
28 J. Y. Fu, P. Y. Liu, J. Cheng, A. S. Bhalla and R. Guo, *Appl. Phys. Lett.*, 2007, **90**, 212907.